MAX-PLANCK-INSTITUT FÜR PLASMAPHYSIK

GARCHING BEI MÜNCHEN

Cs^+ Ion Source for Secondary Ion Mass Spectrometry

B.L. Bentz, H. Weiß, and H. Liebl

IPP 9/37 December 1981

Die nachstehende Arbeit wurde im Rahmen des Vertrages zwischen dem Max-Planck-Institut für Plasmaphysik und der Europäischen Atomgemeinschaft über die Zusammenarbeit auf dem Gebiete der Plasmaphysik durchgeführt.

IPP 9/37

B.L. Bentz, H. Weiß,
and H. Liebl

Cs^+ Ion Source for Secondary Ion Mass Spectrometry

Abstract

Various types of cesium ionization sources currently used in secondary ion mass spectrometry are briefly reviewed, followed by a description of the design and performance of a novel, thermal surface ionization Cs^+ source developed in this laboratory. The source was evaluated for secondary ion mass spectrometry applications using the COALA ion microprobe mass analyzer.

Cs^+ Ion Source for Secondary Ion Mass Spectrometry

I. INTRODUCTION 1

A. General Remarks 1

B. Cesium - The Element 2

II. MECHANISMS FOR ENHANCED SECONDARY NEGATIVE ION YIELDS 4

III. SIMS PRIMARY ION SOURCES UTILIZING CESIUM 5

A. Transmission Surface Ionization Method Using Porous Ionizer 6

B. Other Methods 10

1. Laser Photoionization Source of Cs^+ 10

2. Flooding the Sample with Neutral Cesium Atoms Coincident with Inert Gas Ion Bombardment 10

3. Liquid Metal Field Ion Source 11

C. Surface Ionization Source Featuring a Non-porous Emitting Surface 13

1. Source Design 16

2. Experimental Data and Discussion 21

IV. CS-BOMBARDMENT NEGATIVE-ION SIMS USING THE *COALA* ION MICROPROBE 25

A. Instrument Description 25

B. Instrument Performance 29

V. REFERENCES 37

I. INTRODUCTION

A. General Remarks

Although a number of gas discharge type primary ion sources (1) is being used today in secondary ion mass spectrometry (SIMS) (Finkelstein, r.f., duoplasmatron, Colutron), the duoplasmatron continues generally to serve as the "old faithful", workhorse analytical ion source. This is due to its proven stability of extracted ion currents, and to the multiplicity of charged particle types (+ and - ions, polyatomic ions, multiply charged ions) which can be generated in its gas discharge under various operating conditions, thus allowing convenient selection of bombarding species known to influence the chemistry ensuing during the primary ion - solid target interaction. Although the detailed mechanisms of this physico-chemistry are presently neither clearly understood nor actively investigated, a judicious choice of projectile - target combination can afford selective enhancements of secondary ion signals - an experimental reality which has potential to open a wide and dynamic field for both experimental and theoretical development. Recently, surface ionization type sources to produce beams of Cs^+ have received increasing interest because enhanced secondary negative ion emission results for a number of elements of analytical interest; hydrogen, the noble metals, and the elements of Group V, VI, and VII are cited as relevant examples (2). From an analytical standpoint, enhanced negative ion yields give the practicing spectroscopist expectation of improved detection sensitivities. Furthermore, for a given ion count, sample consumption is less which implies that depth profiles can be obtained from smaller areas. It has been nearly 19 years since Krohn's first published SIMS work with Cs (3), and in the following time until present, a number of technological improvements and modifications in source designs have been described. Similarly, many analytical applications (depth profile measurements, trace element analysis) have been reported using Cs^+ sources. Therefore, this brief report is intended to

(a) serve as an up-dated reference list, data base, and/or condensed literature review of Cs sources applied in SIMS

(b) present an "actualized" laboratory report concerning the design, evaluation, and applications of a Cs^+ source developed in our laboratory at IPP.

It is anticipated that the information disseminated here will provide the reader a brief, concise, and informative overview of Cs Ion Sources applied in SIMS.

B. Cesium - The element

(1) General Physicochemical Data

at. wt.: 132.90, monoisotopic
at. no.: 55
mp.: 28.4° C
bp.: 678° C
density: 1.87 g/cm^3
IP.: 3.88 eV
valence: 1
color: silvery metal
alkalinity: most electropositive and most alkaline element
ΔH(ads): 2.8 eV
ΔH(vap): 0.7 eV
ionic radius: 1.69 Å

atomic diameter: 5.4 Å
IP.(II): 25.1 eV
work function: 2.14 eV

(2) Oxide Forms

Cs oxide (Cs_2O): orange needle-like structure, very soluble in cold H_2O. d 400° C.

Cs peroxide (Cs_2O_2): pale yellow needle-like structure, soluble in cold H_2O, decomposes in hot H_2O, soluble in acid. mp 400° C.

Cs trioxide (Cs_2O_3): chocolate brown color, decomposes in cold H_2O, soluble in acid. mp 400° C.

Cs hydroxide (CsOH): light yellow color, very deliquescent, soluble in alcohol. mp 273° C.

Heat of formation of cesium inorganic oxides: see Table 1a.

$2\,Cs(c) + 1/2\,O_2(g) = Cs_2O(c)$	(298.16°–301.5°K.)	−75,900
$2\,Cs(l) + 1/2\,O_2(g) = Cs_2O(c)$	(301.5°–763° K.)	−76,900
$2\,Cs(l) + 1/2\,O_2(g) = Cs_2O(l)$	(763°–963° K.)	−75,370
$2\,Cs(g) + 1/2\,O_2(g) = Cs_2O(l)$	(963°–1,500° K.)	−113,790
$2\,Cs(c) + O_2(g) = Cs_2O_2(c)$	(298.16°–301.5° K.)	−96,500
$2\,Cs(l) + O_2(g) = Cs_2O_2(c)$	(301.5°–870° K.)	−97,800
$2\,Cs(l) + O_2(g) = Cs_2O_2(l)$	(870°–963° K.)	−96,060
$2\,Cs(g) + O_2(g) = Cs_2O_2(l)$	(963°–1,500° K.)	−134,000
$2\,Cs(c) + 3/2\,O_2(g) = Cs_2O_3(c)$	(298.16°–301.5° K.)	−112,690
$2\,Cs(l) + 3/2\,O_2(g) = Cs_2O_3(c)$	(301.5°–775° K.)	−113,840
$2\,Cs(l) + 3/2\,O_2(g) = Cs_2O_3(l)$	(775°–963° K.)	−110,740
$2\,Cs(g) + 3/2\,O_2(g) = Cs_2O_3(l)$	(963°–1,500° K.)	−148,680
$Cs(c) + O_2(g) = CsO_2(c)$	(298.16°–301.5° K.)	−63,590
$Cs(l) + O_2(g) = CsO_2(c)$	(301.5°–705° K.)	−64,240
$Cs(l) + O_2(g) = CsO_2(l)$	(705°–963° K.)	−61,770
$Cs(g) + O_2(g) = CsO_2(l)$	(963°–1,500° K.)	−80,500

Table 1a: Heat of formation of cesium inorganic oxides. Values given in units of gram calories per mole

(3) Other Facts

Human toxicity:	low, generally nontoxic to humans, can act as an analog of K and thus be potentially harmful (Merck Index)
Fire hazard:	dangerous, reacts explosively with cold H_2O or moist air
Cost:	$ 20/gram
Temperature dependence of Vapor Pressure:	see Table 1b
Source:	occurs in lepidolite, pollucite

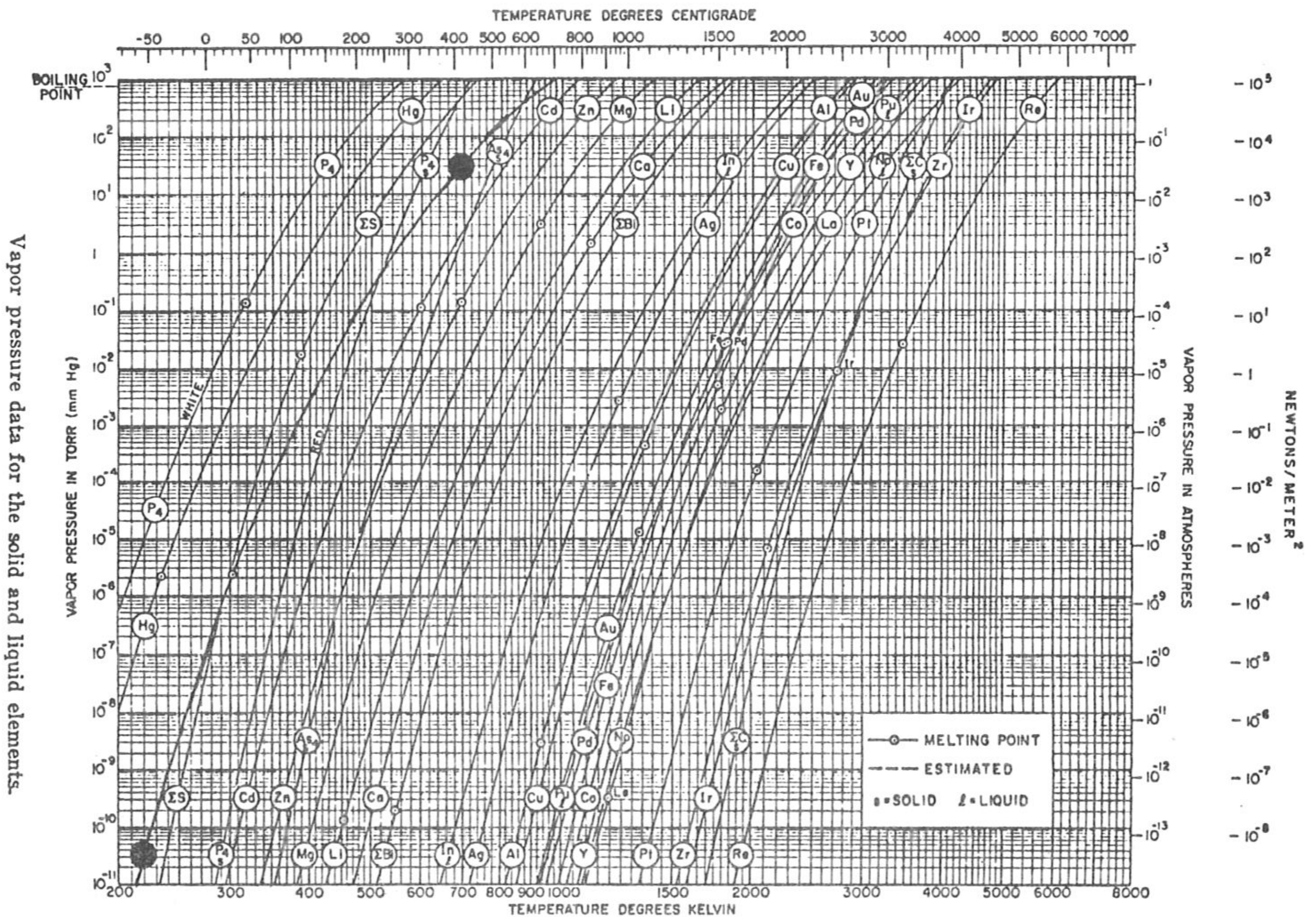

Table 1b: Cesium vapor pressure as a function of temperature

(4) Discussion

Cesium is a chemically active metal and requires carefully performed hermetic sealing procedures (vial loading in a glove box). At all times, the metal should be stored in vacuum or in an inert gas atmosphere. Under the temperature conditions of our ion source, cesium does not react chemically with Re (filament material), nitrogen (source venting gas), or the tantalum comprising the source anode. Probably the greatest potential threat to poison the ionizer is the formation of stable cesium oxides. Condensation of Cs vapor on HV electrical feedthroughs must also be avoided. The warning to flammability is to be heeded: a small explosion with fire was once experienced when the source was incorrectly handled and vented!

II. MECHANISMS FOR ENHANCED SECONDARY NEGATIVE ION YIELDS

One can read in the SIMS literature that Cs^+ bombardment or Cs flooding enhances the negative ion sputter yield of the electronegative elements. Yet, a paucity of data exists as to the degree of absolute ion sputter yield enhancements under saturation conditions (Baril reported an ionic efficiency for Cu^- at 10^{-4} (4), Krohn reported yields of 1 % (3)). What is reported more commonly are "relative" secondary negative ion yields (2); i.e., the pulse counting rate of detected ions, normalized to a criterion of incident-nA Cs^+ target current. These values may be heavily system dependent. Therefore, a better description is "transmission-yield". For example, Storms reported (2) a value for Cu^- of 1.5×10^4 cps/nA, or equivalently 2.4×10^{-6} Cu^- ions detected per Cs^+ primary ion. Absolute neutral atom sputter yields of several metals (Al, Ti, Fe, Cu) subjected to Cs^+ bombardment have been measured (5). Abdullayeva et al. have measured the dependence of the neutral atom sputter yield of Cu, the copper negative secondary ion sputter yield, and the relative ionization efficiency β^-; all quantities as a function of the Cs^+ bombardment energy (range 500 - 3000 eV) (6). Sodium was deposited simultaneously during the sputtering. Their results show that β^- (as high as 10 %) is dependent only to a small extent on the energy of the primary ions and grows slightly when the energy of the incident ions is reduced.

As a result of energetic ion bombardment, it is recognized that a buildup of implanted concentration of primary beam species exists under the sputtered surface. One report found that surface cesium concentration increased with increasing inverse sputter yield of the substrate (7). At thin coverages, Cs atoms absorbed on metal surfaces possess a positive time-averaged charge. These charges together with their mirror images form an electric double layer on the instantaneous surface which lowers the effective work function of the absorbent. Bernheim et al. have recently published a nice work in which both the Cu^- secondary ion signal and surface work function change were monitored as a pure Cu single crystal was flooded with cesium vapor (8). At the cesium coverage (oven temperature was the true parameter) which rendered a minimum in the work function change, it was noted that the Cu^- signal reached a maximum. That yields of secondary negative ions are enhanced may be due to a mechanism that of a surface ionization type, in which the negative ion formation is related both to the decreased effective work function of the material to be sputtered, and to the intrinsic positive electron affinity of the sputtered metal atoms. A theory has been proposed which includes these parameters (9), but more work needs to be done before any definite statements can be made regarding ionization processes.

III. SIMS PRIMARY ION SOURCES UTILIZING CESIUM

Probably one of the most primitive (but effective nonetheless) source designs was Andersen's thermionic unit (9), wherein a cesium compound was simply deposited onto a tungsten filament which was subsequently resistively heated. Such a design may be termed a "unifilar" source (10), refering to the method in which a single heater is used to produce the vapor of Cs and to ionize it. Serious drawbacks of this source are the impossibility of separate control of the amount of material being evaporated and of its degree of ionization, in addition to low output (emittance) and short lifetime. However, analytical results obtained with this source (9) were sufficiently encouraging to stimulate other researchers to develope more versatile sources. One such source, described by Okano in 1972, formed a Cs^+ population by heating Cs_2CrO_4 in a nickel oven (9a).

A. Transmission Surface Ionization Method Using Porous Ionizers ("Contact" Ionization)

The first significant publication to report details of source fabrication and operation was presented by Williams et al. (11). Figure 1 shows the Cs source, now commercially available as the "System 133 Cesium Ion Source" from General Ionex Corp., 19 Graf Road , Newburyport, Ma 01950 (cost $\sim$ $ 30,000). The technology involved in

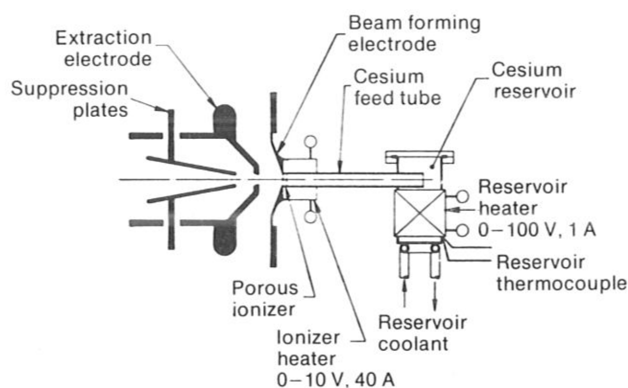

Fig. 1: Cs Ion Source described by Williams et al. (11)

fabricating this source was heavily borrowed from earlier, well-developed proposals to use a Cs surface ionization source as a space ion thruster. Cesium metal is vaporized in a stainless steel reservoir which is maintained at 260^0 C (cesium vapor pressure at 533 K $\cong$ 1 Torr), and diffuses via a molybdenum feed tube to the rear of a porous tungsten frit which is maintained at 1100 - 1200^0 C. Upon diffusing through the frit, the cesium atoms leave the W surface as ions (the *surface ionization* process, as described in

(a) Atom and Ion Sources, L. Valyi, John Wiley, Budapest, 1977, Chapters 1 and 3

(b) Surface Ionization, Zandberg and Ionov, Israel Program for Scientific Translations, Jerusalem, 1971

(c) Ion Beams with Application to Ion Implantation, R. Wilson and G. Brewer, John Wiley, New York, 1973, Chapter 1).

Table 2

Lab., System	Primary Beam Energy	Beam Current delivered to Target	Beam Diameter	Current Density	Stability	Lifetime	Comments	Reference
EVANS and Williams General Ionex Model 133 Source on AEI IM 20	+ 15 KV to 20 KV	65 nA under optimum conditions	minimum 8μm 20 μm-30 μm	20 mA/cm^2 max. 10 mA/cm^2 routine	After 1 hr warm-up, 1 % over 1 hr.	5 g. should last 1000 hrs.	Source mounts on 8" flange. Power requirements for reservoir = 40 W; for frit = 350 W. noted formation of sputtered neutral films inside the extraction electrode assembly of the primary ion column.	11
MAGEE, Colutron gun modification on RCA's SIQMS instrument	+ 5 KV (60°)	200 nA	70 μm	5.2 mA/cm^2	sputter rates are stable to ± 2 %/day		Source mounts on 2.75" flange.	24, 28
STORMS, Hughes Res.Lab. source on ARL IMMA	+ 15 KV	total current output from source = 35 μA 3 nA typical	minimum 1-2 μm	.1-.2 mA/cm^2 defocused $\approx$ 30 mA/cm^2 focused	± 1 % in 20 min. Sudden "shifts" often observed	$\approx$ 300 hrs	ion source start up and shut down requires 2 hrs. for one complete cycle.	2
VALLERAND & BARIL, homemade system	+ 5.5 KV + 5.5 KV	500 nA 1 μA	.78 mm 2.03 mm	100 μA/cm^2 30 μA/cm^2				4, 34

A comprehensive theory for the working of a porous ionizer has recently appeared (12). Porous tungsten frits may be purchased from Metallwerke Plansee, Reutte, Tirol, Austria, or from Spectra-MAT, Watsonville, Ca. A number of publications summarize experiments in which this source was employed; more information may be found in references 13-21. Relevant source features and typical SIMS operating conditions are listed in Table 2.

Hughes Research Laboratory has designed and constructed a cesium positive ion source (shown in Figs. 2a and 2b), and Storms et al. have evaluated analytically this device for SIMS applications (2, 22). The

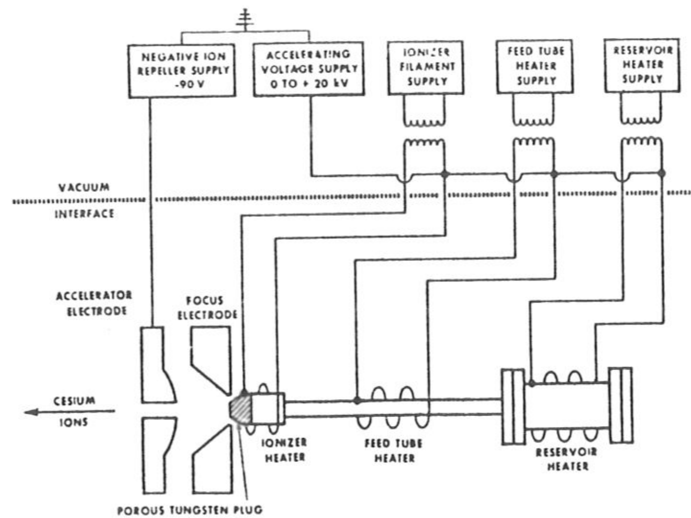

Fig. 2a: Cs positive ion source described by Storms

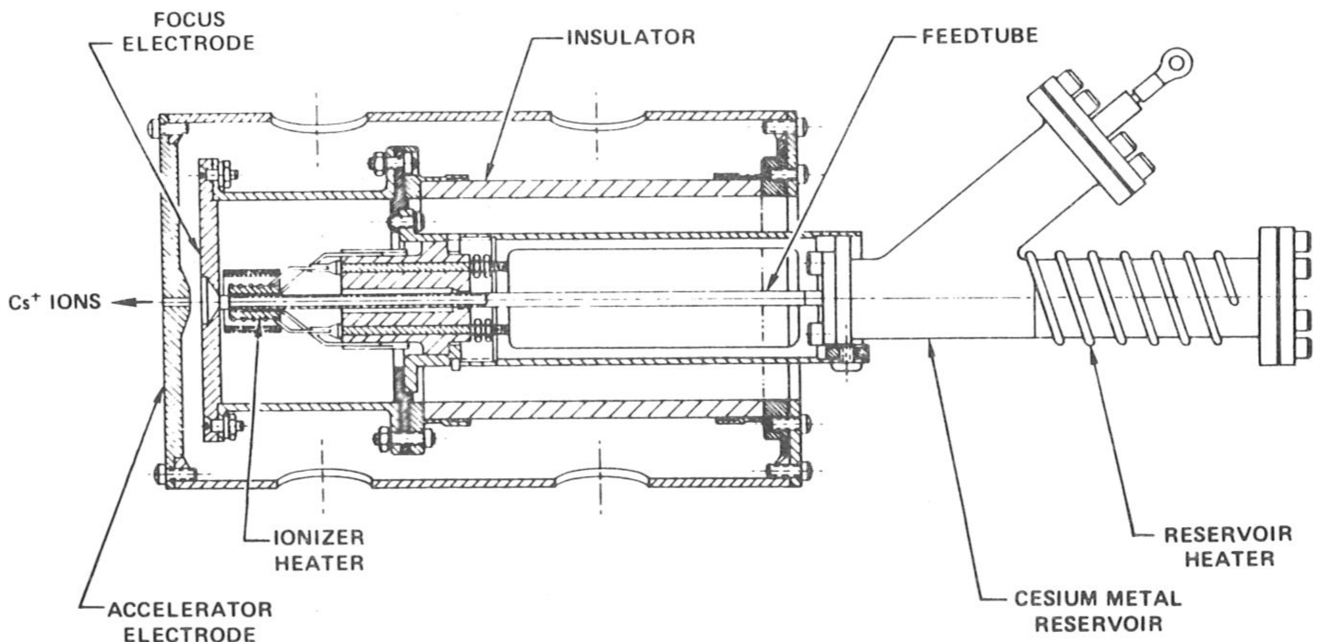

Fig. 2b: A more detailed view of the device used by Storms

ion source is approximately 75 mm in diameter and 225 mm long. A hot, porous tungsten plug serves again as the ionizing surface. Cs ions generated at the front surface of the plug are accelerated into the ion probe by the potential difference between the plug and the acceleration electrode. Operational details may be found in Table 2. Consideration was once given to make the source commercially available, but later withdrawn due to anticipated high production costs.

A Cs ion source - quadrupole SIMS system has been developed by Magee at RCA. Construction of the Cs source is a low cost, straightforward alteration to the Colutron argon ion source normally used on his instrument (23). The relevant modifications entail a W frit (1 mm effective diameter) pressed into the end of a Mo tube which is heated to 1100° C by the existing filament of the Colutron source (a dc arc, 0.03 Torr discharge type source) (24). Under the conditions of his primary ion optics, Magee's gun can deliver 200 nA Cs^{+} (E x B mass filtered) into a 70 μm diameter probe spot (i.e. $\approx$ 5 mA/cm^{2}) at 3-5 KV. This yields a 5 Å/sec sputtering rate in Si when rastering over a 700 x 700 μm^{2} area. The incorporation of an isolation valve between the source and the main vacuum chamber assists rapid interchange ($\approx$ 30 min. system down-time) of Cs/Ar sources. True UHV conditions($\approx$ 10^{-10} Torr) are maintained in the sample vicinity. This system is probably the foremost available presently for H analysis (25). Applications using this system are given in references 26-33.

Baril and Vallerand have assembled a SIMS system which employs a thermionic Cs primary ion source (3, 34). Published details on their source design are limited (independent pumping of source from target chamber, neutral cesium beam dump), but some relevant operating conditions are listed in Table 2. Applications have included sampling steels with interest in computer modeling of secondary ion mass spectra, and also a general study for cluster ion formation (35-37).

B. Other Methods

1. Laser Photoionization Source of Cs^+

A system has been described recently whereby a Cs atomic beam is partially converted into a Cs ion beam by a resonant two-photon absorption process using photons produced by a cw laser (38). This rather complex and expensive ionization unit, proposed as a charged particle source for ion microscopy, has a measured source brightness of 10^{-4} A/cm^2·sr·eV. The author recognized that this brightness value was significantly too low to be useful, and later discussed improved experimental conditions on this same system which, (1) increased the Cs^0 ionization probability from $\sim 10^{-4}$ to > 0.1; and (2) increased the brightness to 0.24 A/cm^2·sr with a $\Delta\varepsilon$ value of 0.09 eV (39). That this value is still low suggests very limited future practical employment of this source to SIMS.

2. Flooding the Sample with Neutral Cesium Atoms Coincident with Inert Gas Ion Bombardment

The methodology involves directing a collimated cesium vapor jet, issuing (say) from an electron beam heated (40) reservoir containing a cesium alkali metal salt (CsI) placed in the target chamber, onto the analytical sample-target simultaneously subjected to energetic noble gas ion beam bombardment (41). A Knudsen cell filled with pure cesium metal has also been used as an atomic beam source (42). Alternatively, a heated cesium dispenser containing a mixture of cesium chromate and a reducing agent can generate a flux of cesium neutrals (42), but most likely with concomitant hydrogen impurity release into the vacuum vessel (43). Reported advantages of this procedure to introduce cesium to the surface as opposed to the method of implanting reactive atoms by means of the bombarding ion beam include

(a) the latter method can lead to superficial layers which are not saturated by reactive atoms (44, 45)

(b) the possibility exists to control the Cs coverage independently of the sputtering yield (8).

Special attention must be given to: stability of the neutral flux, collimation of the neutral beam, and securing that the density of the cesium atoms impinging on the sample surface is well correlated to the primary ion current density. At present, it can be stated that the weakness of the cesium flux is not compatible with high sputtering rates (46). Cesium migration is also a problem, particularly if the sputtered area is smaller than the deposition area.

3. Liquid Metal Field Ion Source

In principle, this class of ion source, with its reported high brightness (47), appears to offer the ion microscopist the capability of high resolution (sub 1000 Å - 1000 Å) SIMS microanalysis, although few literature citings describe actual SIMS applications. Rather, results of prototype sources coupled to test pump benches have indicated beams of liquid gallium (47-54), cesium (47, 55), mercury (47), bismuth (49), gold (51, 53, 56, 57), arsenic (58), and silicon (58), are able to be formed, albeit with some experimental difficulties and complexities which may preclude their widespread employment in the general laboratory. Figure 3 shows a simplified schematic of a liquid metal field ion source. Essential to the realization of tight, high current microbeams are optimized beam optics and lens designs (59), a fact which may not be generally

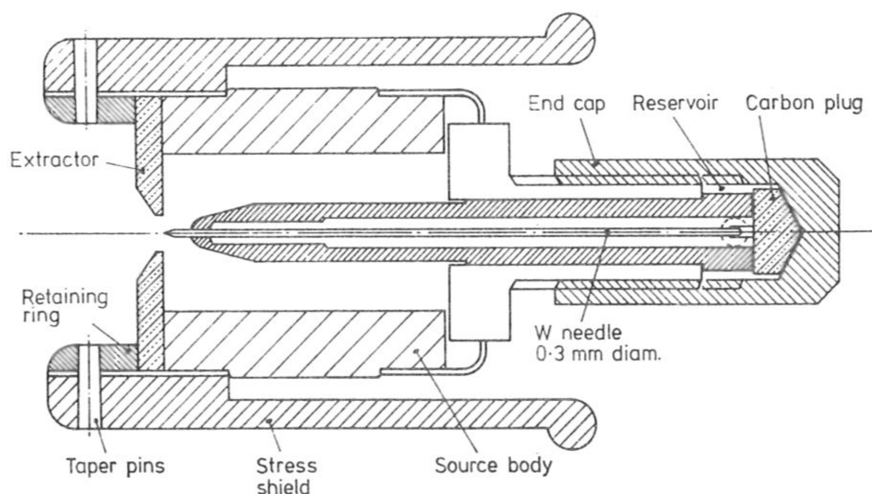

Fig. 3: A Ga EHD positive ion source (53)

recognized. The point of concern is that, contrary to the conventional case in ion microprobes, the electrostatic lenses are not to form a strongly demagnified image of the virtual source, because the virtual diameter of a LMFIS amounts to a few nanometers at most (59). The source lens should have a very short focal length comparable with that of the objective lens, so that the imaging ratio is not too different from unity (59). At 21 KV, a device feeding liquid Cs showed a brightness of 1.8×10^4 $A/cm^2 \cdot sr$ (47) notwithstanding the fact that a hammer tap (yes, a hammer!) may have been necessary to ensure stable current production! Dubilier Scientific Ltd. of Abingdon, England, has recently marketed a metal ion source which uses cesium as emission material. Electrical specifications are given as 0.1 - 10 keV beam energy, > 10 µA/sr beam angular intensity with beam current stability over 2 hours of 1 % or better (60). It is noted that the preferred mounting orientation of the source is vertical, which may be a severe constructional limitation in some systems. More recently, test results of a commercially available Ga^+ source (reported merits of 0.5 nA into 5000 Å at 10 kV) have appeared (61). As one of the first true applications of LMFI sources to SIMS, this Ga^+ source has been used to map the Al distribution on part of an integrated circuit (analytical secondary ion: $^{27}Al^+$) (51, 61). Whether Charles Evans' comment at the 2nd Japan-USA Joint Seminar on SIMS (Takarazuka, Japan 1978) of "I do not think the EHD will become a useful ion source for SIMS in the near future" is a true prophecy or not remains to be seen. Commercial interests in producing submicron ion beams for circuit writing and micromachining may, in the future, lead to developments which might challenge this statement. To date, liquid metal field ion sources do offer high brightness, but suffer from the disadvantage that the ion beams produced are multicomponent in that singly charged, multiply charged, and cluster ion species are observed (58). One noteworthy comment: a primary ion optical column incorporating a liquid metal field ion source plus optimized lens designs has potential to yield high current density, sub-micron diameter primary beams, a factor which is important when high throughput, micromachining is the task at hand. To be analytically advantageous in SIMS however, it will be necessary to measure neutral atom sputtering yields, and especially positive and negative ion secondary ion yields, of the elements when they are sub-

jected to bombardment by ions produced from this class of source. One first step in this direction has recently been made by Rüdenauer (62). Using an EHD-type In ion source, secondary positive ion "useful" yields have been measured. Compared to O_2^+ bombardment, yield results for pure element samples are generally lower by one order of magnitude (62). No data is available with respect to negative secondary ion yields.

C. Surface Ionization Source Featuring a Non-Porous Emitting Surface

One ion-optical aspect of the type of Cs sources depicted in Figs. 1-2, in which ion emission occurs from a planar, porous metal frit, is that the current density at the source is space-charge limited according to Child's law (63)

$$J = \frac{5.45 \times 10^{-8}}{\sqrt{M}} \frac{V^{3/2}}{d^2} \ A/cm^2$$

where d = accelerating distance (cm)
V = extraction voltage (V)
M = mass number.

Space charge effects can further limit brightness by increasing the divergence of the beam. Apart from these aspects, the stability and durability of the pores may become questionable at high temperatures (64).

One goal in our ion source development program was to develop a Cs source in which space charge effects are minimized, and which provides higher saturated ion emission current densities than available from planar plug sources. When such an improved bright source is coupled to an ion microprobe incorporating low aberration ion lenses, relatively higher primary beam currents can be focused into smaller spots. This has important implications to the ion microprobe approach to SIMS, particularly for the prospects of approaching very high lateral resolution (sub-micron) while maintaining high sputter rates. Our sources were conceived to be advantageous also in terms of compact design package, low power requirements, and low cost.

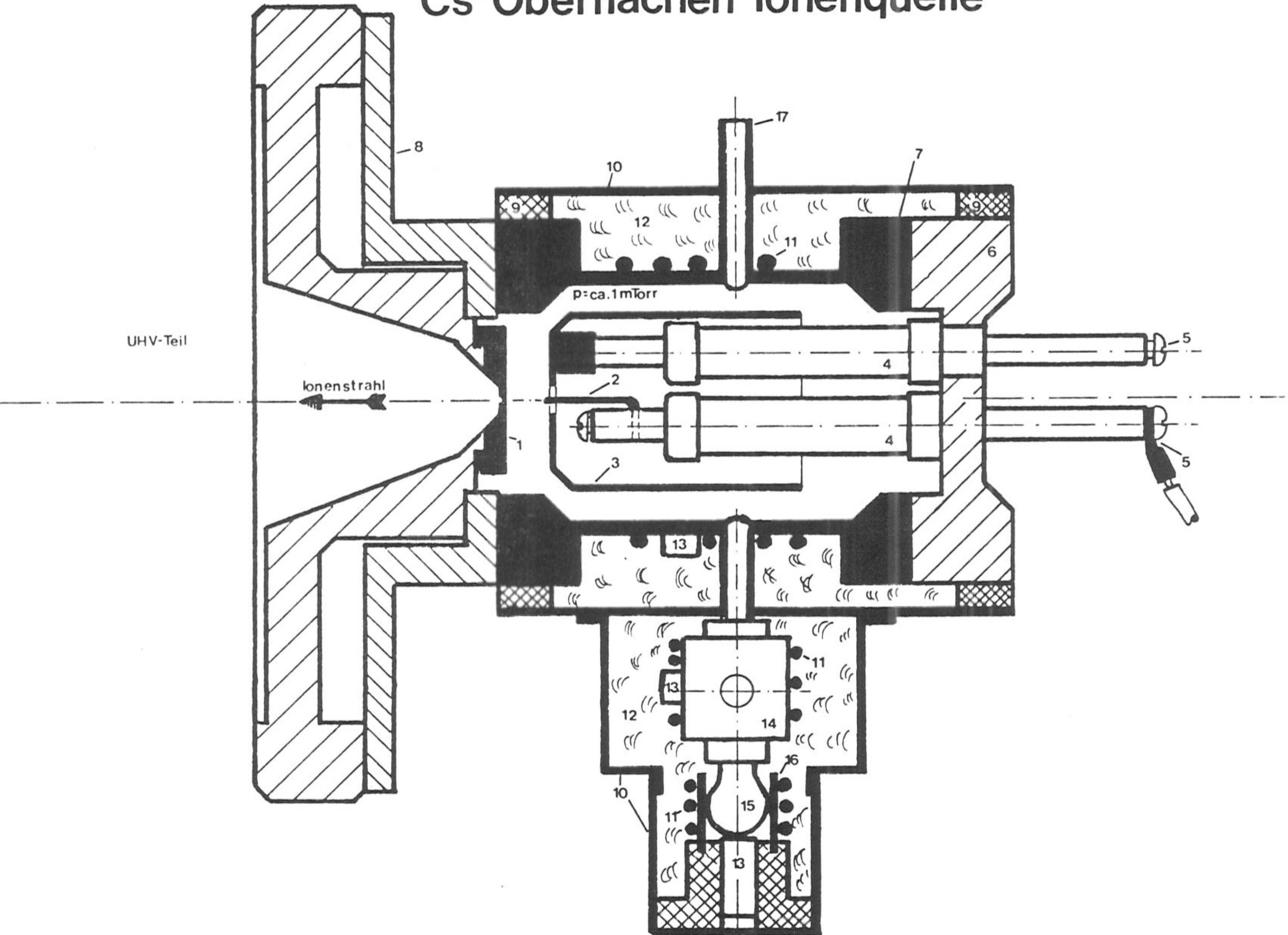

Fig. 4: Ion Source generating $^{133}Cs^{+}$ by surface ionization

Currently in our mass spectrometry laboratory, three differing models of Cs^+ ion sources are being tested, and one of them (65) is operated routinely on the COALA ion microprobe (66). The remaining two are assembled to test pump benches for preliminary evaluation. All three sources were developed by H. Liebl. Figure 4 presents the "Model I" Cs ion source. A concise description of its basis of operation (see Fig. 5 for details) follows:

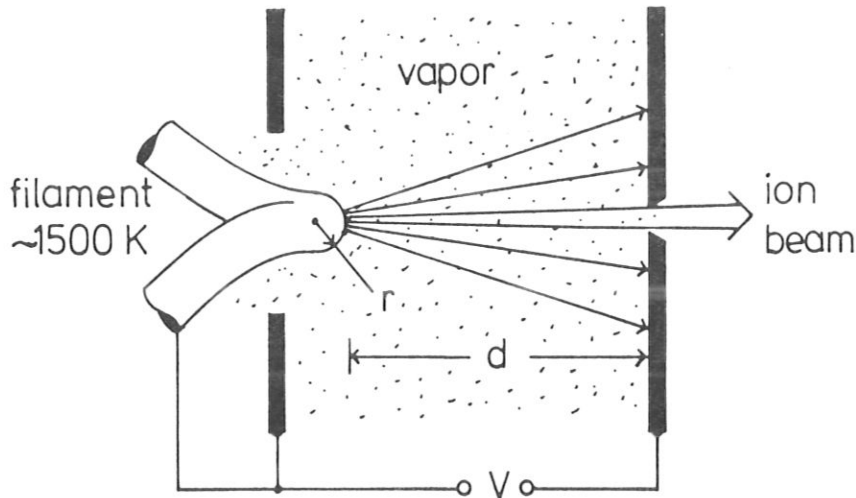

Thermal surface ionization source

Fig. 5: Another view of source depicted in Fig. 4. Parameters are defined in the text

A resistively heated, polycrystalline Re (W = 4,96 eV) cathode having a near spherical tip of radius r is separated from the acceleration electrode by a distance d ($d \gg r$; thereby, the effective accelerating distance being of the order of r). The neutral Cs atom vapor pressure in the ionization chamber is regulated at a value such that the Cs-Cs mean free path corresponds approximately to the distance d. With $0.5\ \text{mm} > r \ll d$, $V > 5$ kV, the emission current density is not limited by space-charge but by vapor density. With $r > 10\ \mu\text{m}$, field ionization is avoided. With $d \approx 5$ mm and conditions as stated above, the saturation current density from the ionizer is about ten times higher than in the planar space-charge limited case. Several important aspects of this source are now described in greater detail.

1. Source Design

a) Ion Source Chamber

With reference to Fig. 4, the ion source chamber /7/ is of V2A steel. It has dimensions 9.1 cm length and 4.3 cm i.d., with an internal volume of 140 cm^3. The chamber is secured to a steel adapter flange /8/ via a 2.75" standard Conflat vacuum flange (Cu O-ring sealed). Another 2.75" o.d. flange /6/ incorporates three HV vacuum feedthroughs /4/ which serve as electrical connections for the dc HV ((+) with respect to ground) to provide Cs^+ ion extraction away from the off-ground filament /2/. This flange is sealed to a vacuum bellows assembly, itself welded to the source chamber, to allow optimum positioning of the filament with respect to a 200 μm diameter orifice located in the grounded anode /1/. The anode is separated from the filament by a distance of $\approx$ 5 mm. The source volume is pumped through the orifice in the anode which has a calculated pumping speed of 1.2 x 10^{-3} l/sec. A Hastings DV-5m thermocouple vacuum gauge attached at port /17/ allows source background pressure monitoring. When assembled on the COALA instrument, the source pressure is typically < 10^{-3} Torr. A Nupro H series SS-4H-TSW bellows valve /14/ serves to isolate the Cs vial /15/ from the source chamber.

The entire chamber is heated near uniformly with resistively heated bands /11/ to a constant temperature of $\approx$ 200° C. An alternative unit to provide local heating could be a heated oil bath circular, but the heating band approach was found to be less complex. Pt 100 thermoresistors /13/ measure various surface temperatures. Thermal shielding is provided by a glass-wool material wrapped around the chamber.

b) Considerations in the Selection of the Anode Material

In order to prevent excessive Cs condensation on the anode surface, the flange /8/ surrounding the anode is heated (with a 600 W heating band) to a temperature equal to or greater than the tempera-

ture of the Cs reservoir. Typically a temperature of $\approx 160^{o}$ C is maintained. In the design of the "Model I" source, the grounded anode is inherently subjected to bombardment by Cs ions desorbed from the hot filament held at KEV potentials, as the anode functions as the first stage acceleration electrode. Consequent to this bombardment, sputtering will occur, and consideration should be given to the selection of anode material for reasons including:

Neutral atom sputtering yield (Y^{O}) of the anode material:
It is desireable to minimize the amount of material which sputtering physically removes from the anode. That material which is removed can agglomerate to form flakes or deposits on the filament, electrical feedthroughs, etc. This has potential to cause accelerating voltage instability (flickering), shorted acceleration gap, and/or work function changes of the filament. In this regard, a protective metal cap /3, Fig. 4/ surrounds the filament and is held at a common potential. Anodes have been machined using V2A steel and Ta. Literature data reveals that Y^{O} (ss) $\cong$ Y^{O} (Ta) $\cong$ 5 by 5 kV Cs^{+} projectiles (5).

Secondary Negative Ion Yield (Y^{-}) of Anode Elemental Constituents:
Secondary negative ions of the anode material (and contaminant species thereon) can be sputter released from the anode, and accelerated to the filament and protective shield-cap by the (+) high voltage applied. Physical sputtering of the latter two source components by these agents is possible, although a visual check of the front surface of the cap reveals no damage. The current carried by these ions may contribute to the standing current measured in the HV acceleration circuit. Data from Storms (2) indicates $Y^{-}_{Fe}/Y^{-}_{Ta} = 7$. Absolute negative ion yields may be in the 10^{-4} - 10^{-3} range.

Secondary Electron Yield:
Little work has been done to obtain secondary electron emission coefficients of Ta and stainless steel, particularly under Cs bombardment. Many metals which have a thin layer Cs coverage exhibit increased secondary electron emission. For example, a factor of 3.5 increase in the secondary electron yield has been measured for 5 kV Cs^{+} ions incident on cesiated W compared to clean W (67). Secondary electrons

produced as a result of the sputter process will reach the ion emitter—cap assembly and contribute to the total standing current measured in the HV acceleration circuit.

The 200 μm diameter orifice drilled in the anode has never been observed to be fully plugged, although sometimes heavily occluded. A simple re-drilling of the hole renews the anode. After 110 hours of 5 kV Cs^+ ion bombardment at 1mA circuit current levels using a Ta electrode, a 47 mg weight gain of the protective cap was measured. This contamination poses no major problem as long as it doesn't interfere with acceleration voltage stability. It is to be noted that an acceleration-extraction electrode in other style Cs^+ ion sources will be subjected to similar sputtering and flaking problems (see Table 2, Comments section).

c) Filament Geometry

The filament's preferred radial dimensions in this device have been described in III.c. We have experimented with two filament configurations; one with a hairpin geometry and, less extensively, with a filament assembly incorporating an electrolytically etched tip. In the former design, a polycrystalline Re wire of diameter 0.6 mm is bent into a hairpin shape, the tip of the "hairpin" being roughly V-shaped projecting an ellipsoidal apex (68). Tungsten could as well serve as filament material in a Cs ion source; a comparison of W with Re reveals that (1) Re has a higher work function than W by $\approx$ 0.4 eV, (2) at equal temperatures, the evaporation rates of W and Re are not greatly different (Re at T = 1000^{0} C has a vapor pressure of $\approx 10^{-19}$ Torr (10^{-19} g/cm^2 sec) and an electron emission value of $\approx 10^{-10}$ mA/cm^2), (3) Re is somewhat less expensive than W. The filament, held at the HV accelerating potential, is resistively heated and dc powered. The resistivity of Re is larger than of W; a filament of a given diameter, therefore, made from Re, requires less current (but higher voltage) to achieve a certain temperature. Re is also more ductile than W. Table 3 presents typical operating power requirements for the filament and other heating units associated with the source. An optical pyrometer is used to obtain a value of the

Table 3: Power Requirements for "Model I" Cs Source

Heater Unit	Nominal Operating Temperature ^oC	Power Utilized (W)	Regulation Mode	Thermo-element Sensor	Tempera-ture Stability
anode	150	(AC) 182	(Variac)	Pt 100	$\pm$ .1-.2 over 24 hours
source chamber	200	(AC) 50	Pantatherm D thermo-regulator	"	"
valve	190	(AC) 10.5	(Variac)	"	"
Cs vial	$\approx$ 150	(AC) 2.5	(Variac)	"	"
filament	900-950	(DC) 8	constant current mode		-

filament spectral temperature. During source start-up on the COALA, the filament is heated at 1200° C for 45 minutes in a vacuum of < 10^{-3} Torr before the Cs valve is opened. This allows sufficient time for the thermal radiation dissipated from the hot filament ($\approx$ 8 W) to uniformly heat nearby internal source parts (especially voltage feedthroughs).

It was mentioned earlier that the tip region of the hairpin type filament has asymmetric geometry. When considered in context with the ion acceleration electric field configured in the near tip region, it is recognized that ion emission with larger angular spread may occur where the electric field is enhanced due to the physical geometry. This effect is indirectly observable as shown in Fig. 6a. This photo-

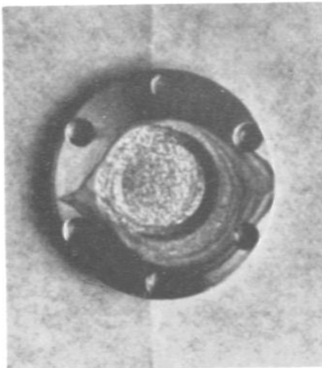

6a

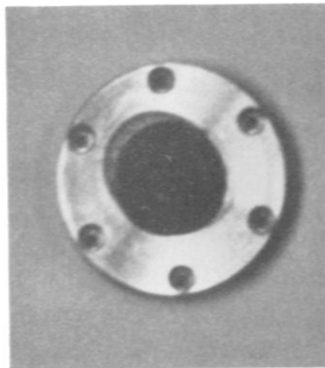

6b

Fig. 6: Photographs of sputter erosion patterns observed using V2A steel anode

graph shows sputter damage evident on a V2A steel anode when a Re hairpin filament was employed. Clearly recognizable in the post bombardment erosion pattern are two "pointed notches" located at the far left and right (somewhat less well defined) along the sputtered area periphery. Directional non-uniformity in surface sputtering is apparent due to electric field inhomogeneity. This is to be contrasted with the erosion pattern observed on another anode of similar material when the second filament style, formed from a short Re wire whose end was chemically etched to yield a nearly spherical top, was tested. This piece was then spot welded to an arc-shaped Re support filament. Figure 6b shows the sputter removal pattern observed under similar experimental conditions. The damage is without local irregularities and appears quite symmetric (round), observations ascribable to improved electric field conditions at the filament tip. For most of the work described in this report, a hairpin type cathode has been used.

d) Cesium Supply Reservoir

Solid Cs metal is stored in a tear-drop shaped Pyrex ampule /15, Fig. 4/. The vial has sufficient internal volume to house 0.8 - 1 gram cesium. No corrosive action on the glass has been observed. The Cs is obtained from Merck, delivered with chemical purity listed as 99.98 %. We have purchased a glove box in which the Cs reservoirs for all three sources can be filled in a positive-pressure argon atmosphere. A heating band /11, Fig. 4/ is used to heat the vial to provide the requisite Cs vapor pressure. The temperature of the vial is measured with a Pt 100 thermoelement /13, Fig. 4/ coupled to a Normatemp D 2401 digital thermometer. From Table 1b, one notes that Cs vapor pressure is a relatively strong function of temperature. If the Cs vapor pressure curve is used in the temperature range 343-423 K, an absolute error of $\pm$ 3 K results in a relative error in the estimated vapor pressure of between 15 - 20 %. The Cs reservoir temperature is kept the coolest relative to the valve and chamber to prevent unwanted distillation into the chamber, and to control the neutral Cs atom incidence rate on the ionizer surface. The main "loss" mechanisms of neutral cesium in this source include Cs atom efflux, under molecular

flow conditions, through the anode orifice, and those Cs atoms lost as ions formed by surface ionization. The following chart presents an inventory of Cs particles:

Cs temperature °C	Vapor Pressure (μm)	Neutral particle flow through the 200 μm diameter orifice (particles/sec)
112	1	7.0×10^{13} (15 ng/sec)
139	5	3.5×10^{14} (77 ng/sec)
150	10	7.1×10^{14} (157ng/sec)

The flow rate loss through the orifice is small, controllable, and amenable to calculation. Additionally, those Cs neutral particles passing through the anode orifice serve as an excellent getter for O_2 and CO (69), thus improving the pressure in the primary ion column on the microprobe. A 1 gram charge has a calculated lifetime over 1000 hours. After several hundred hours of service, it has been noted that an ample supply of metal still remains from an initial charge.

2. Experimental Data and Discussion

Figure 7 shows a representative surface ionization temperature curve obtained at a cesium vapor pressure of 10 microns. The positive ion current was measured at a planar collector without secondary

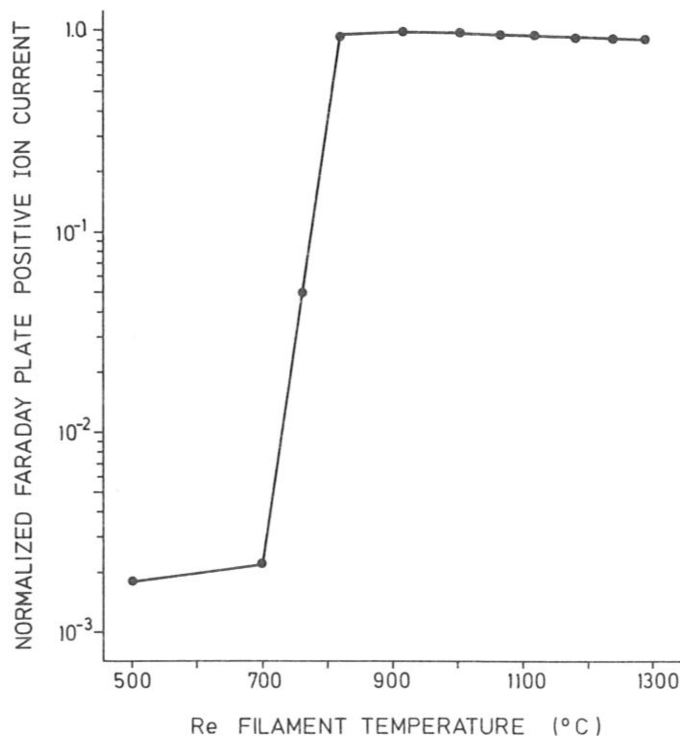

Fig. 7: Beam current-filament temperature characteristic

electron suppression. The following model qualitatively explains the step-like behavior of the ion signal.

The ratio of ionized to total desorbed Cs atoms is given by the Langmuir-Saha law:

$$R_+ = \frac{1}{1 + \omega_+ \exp (I-W)/kT} \quad (\omega_+ = 2 \text{ for Cs})$$

When a Cs atom desorbs from a Cs-covered Re-surface ($I > W$), R_+ is negligibly small. On the other hand, when Cs atoms desorb from a bare Re surface, R_+ is only slightly less than unity ($I-W = -1$ eV) having a weak temperature dependence. Therefore, the ionization ratio averaged over the surface may be considered as the product of R_+ times the ratio R_b of bare to total surface.

The relative coverage of a partly covered surface is given by $\emptyset\sigma\tau$, where $\emptyset$ is the flux of Cs atoms from the vapor phase to the surface (atoms/$cm^2 \cdot s$), σ is the effective cross section of a Cs atom sitting on the surface (cm^2), and τ is its mean sojourn time (s). The latter is given by $\tau = \tau_0 \exp E_d/kT$, where E_d is the desorption energy and τ_0 is a characteristic time related to the lattice vibration period. With that we have $R_b = 1 - \emptyset\sigma\tau$.

Figure 8 shows the general shape of the curves $R_+(T)$ and $R_b(T)$ and their product. The measured curve (Fig. 7) agrees qualitatively with the product curve; even the slight drop with increasing temperature after the flat maximum is visible. Regarding this measurement, several points are emphasized:

(1) ion emission from a porous plug ionizer also exhibits a temperature curve of similar shape, although the mechanistic details differ.

(2) threshold temperatures, or critical temperatures, of porous emitters are known to be higher than for compact metallic surfaces (64), owing to space charge formation in the micron-sized pores. Since the source is normally operated at temperatures somewhat above threshold, an important implication for ion source applications is that the spread in ion energies will be larger using a porous ionizer

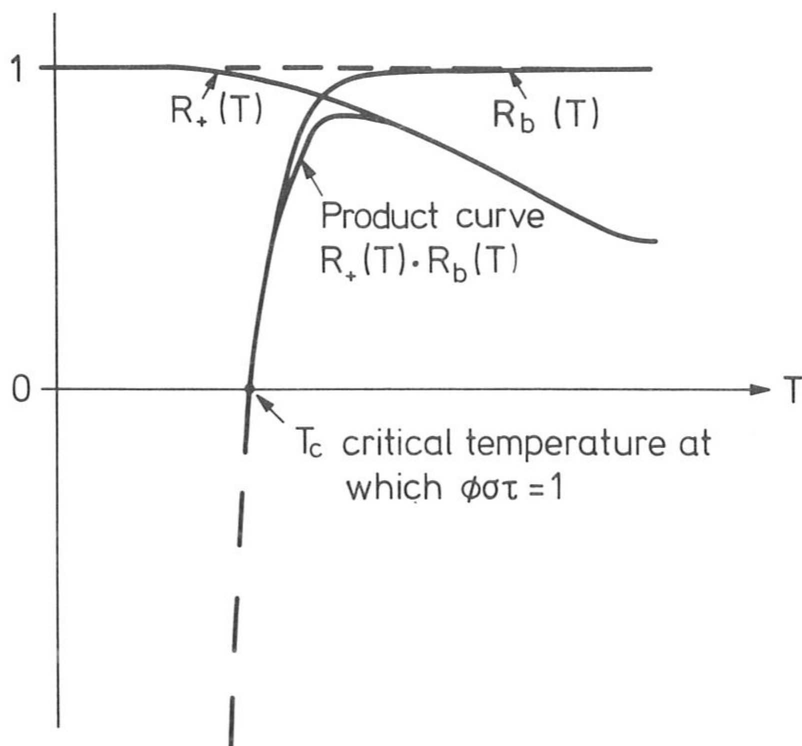

Fig. 8: General slope of the curves $R_+(T)$ and $R_b(T)$

than from a non-porous ionizer. Taking 900^0 C as a surface temperature for stable operation in our source, and assuming a Maxwellian distribution in thermal ion energy, a ΔE value of $\approx$ 0.2 eV is calculated. Compared to beams from a porous W plug said to operate at 1100 - 1200^0 C (2, 11, 24), the ion beams from our source should have a thermal energy spread a factor of 1.2 lower.

A low and high gain (factor 1,000 difference) mass scan of a 5 keV positive ion beam is shown in Fig. 9. With a proper choice of ion-substrate combination and temperature, the surface ionization method can be thought to afford "selective" ionization. Neither ions of the Re thermoemitter proper, background gases in the source chamber, outgassing products, nor impurity ions from the Cs supply are observed. The only signal arises from singly-charged atomic cesium ions. This is not the case with a reported high brightness Cs^+ liquid metal field ion source (70), where cesium cluster ions and cesium oxide species were observed with ratios Cs^+:1, Cs_2^+:0.18, and Cs_3^+:0.07.

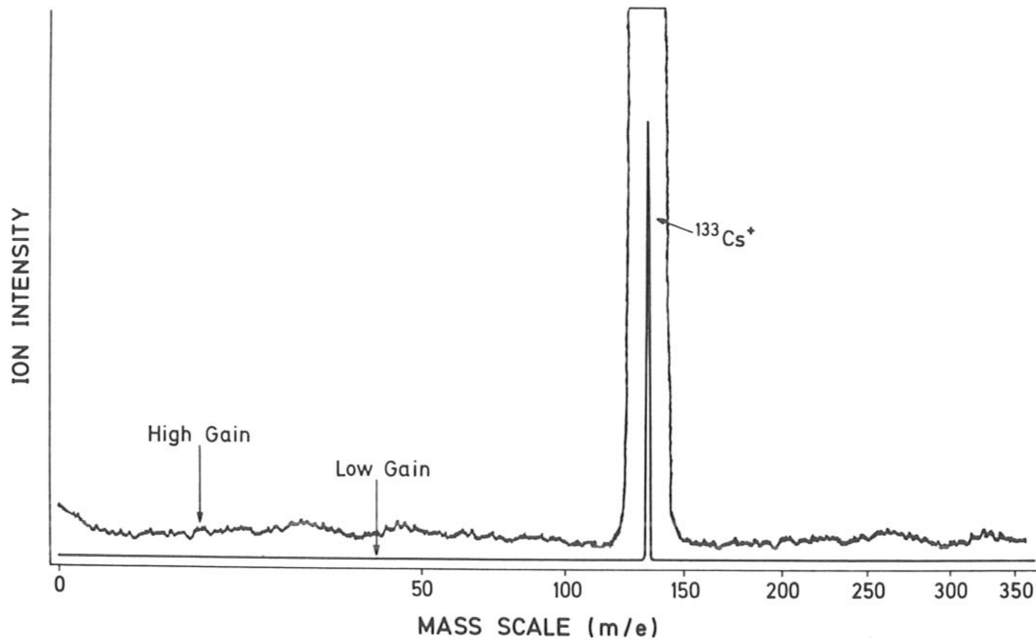

Fig. 9: Ion composition of mass analyzed beam extracted from the source. Note absence of "molecular" species and hydrogenic impurities

Because the beam from our source is highly free from impurities (including hydrogen), it would be ideally suited for use on SIMS machines without primary-ion magnetic mass separation. The liquid metal field ion source will require, at added cost and complexity, primary beam filtering. The source does not produce a gas load into the primary ion column and sample chamber, and thus helps maintain UHV conditions and reduce sample contamination.

In terms of current production, the source at 5 keV accelerating potential easily delivers several tenths of microamperes through the 200 μm diameter orifice. The virtual source size of 20 μm is considerably smaller than values found in SIMS duoplasmatron-type ion source. Beam brightness, measured by the method of rastering a focused beam across a sharp edge, is 33 $A/cm^2.sr$ at 5 keV with T (Cs) = 125^0 C. The measured brightness value is probably biased low compared to the source brightness due to lens aberrations of the imaging system. Measured brightness values for Cs^+ planar plug sources are not available for comparison, although one report comments the brightness to be comparable with a duoplasmatron supplying O_2^+ (beam energy unspecified, (71)). Beam stability is $\pm$ 1 % over 1 hour.

IV. CS-BOMBARDMENT NEGATIVE-ION SIMS USING THE *COALA* ION MICROPROBE

A. Instrument Description

The COALA Ion Microprobe to which the source is coupled (Fig. 10) is similar in design to the UMPA Microprobe described previously (72).

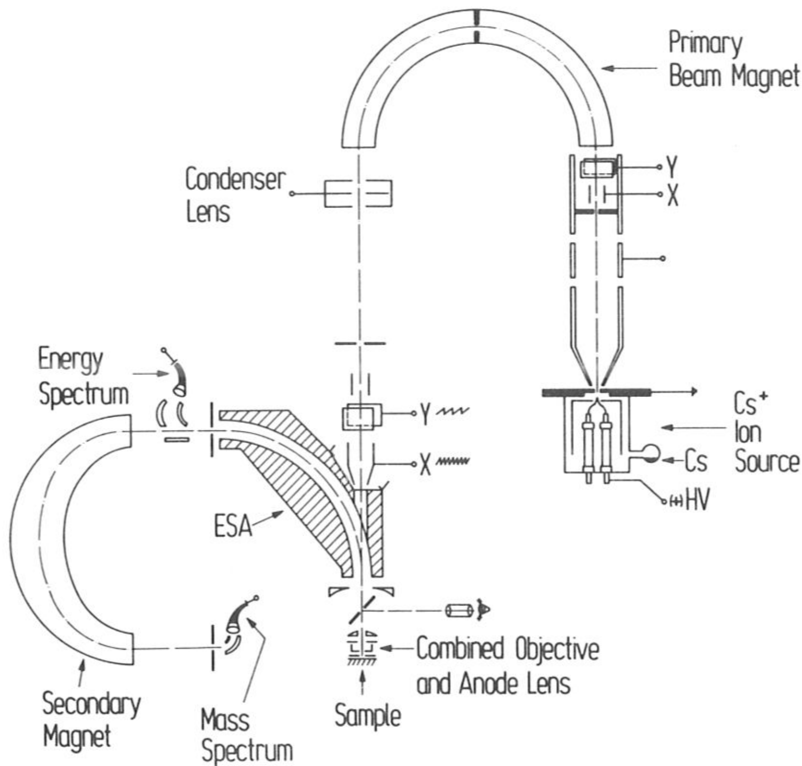

Fig. 10: Schematic layout of ion microprobe

Major modifications are the use of purely electrostatic lenses in the primary beam column (instead of "hybrid lenses") and the COALA lens proper (73), which acts as objective lens to focus the primary beam and as emission lens to accelerate the secondary ions (of opposite polarity) backwards through the lens co-axially with the primary beam.

1. Primary beam column

Ions leave the source as a diverging beam, but an Einzel lens positioned downstream renders the beam parallel for entrance into a 180^0 uniform magnetic field used for primary beam purification. A mass

separating slit is placed in the middle of the half circle, and mass selected ions leave the field again as a parallel beam. This configuration accomplishes mass separation without introducing any lateral probe spot elongation owing to the energy spread of the primary ions (72). Another advantage is that the ion acceleration voltage and the magnetic field need not be extremely constant. The surface ionization Cs^+ source does not require primary beam mass analysis, but when switching over to duoplasmatron operation (with Ar^+, N_2^+, or $O_2^{\pm}$ for (+)ion SIMS), beam purification is needed. The condenser lens controls the beam current delivered to the sample and the overall demagnification from the source to the sample.

After passing the condenser lens and a set of electrostatic deflection plates used for beam adjustment and rastering, the primary beam approaches the last component of the primary ion column, the so-called COALA lens (Combined Objective and Anode Lens Analyzer (73)). This is a three electrode lens arrangement, unique in that by a suitable choice of excitation potentials and primary beam energy, the <u>same</u> set of electrodes simultaneously focuses the primary Cs^+ beam onto the sample and accelerates the negatively-charged secondary ions backwards out of the lens. The two beams of opposite charge polarity thus pass this combined lens coaxially and in opposite directions. This lens design has strong advantages for ion beam microfocusing including (a) an objective lens with short focal length ($\sim$ 6 mm) and small spherical aberration is realized, thereby allowing for a given probe spot size a relatively higher probe current, and (b) a high field strength prevails at the sample surface and therefore better lateral resolution or lower emittance of the secondary beam is provided. The lens assembly incorporates a Schwarzschild-type microscopic objective for viewing the sample *in situ*. Light is delivered to the specimen through a series of bores and by reflection from highly polished integral electrode surfaces. The sample is viewed perpendicular to the surface at a magnification of $\sim$ 150.

2. Sample stage

Samples are mounted on a conducting target platrode, itself assembled to a Vacuum Generators Model HPT high precision XYZ manipulator equipped with "Z" rotation and tilt accessory. Beam current delivered to the sample can be accurately measured by use of a Faraday Cup. The sample is housed in a chamber pumped by a 450 l/sec turbo pump fitted with a coolable sorption trap, a 1600 cm^2 LN_2 cold wall, and a Ti sublimation pump. Pressures in the 10^{-9} Torr range are achievable. An additional LN_2 shroud surrounds the sample to reduce H_2O and hydrocarbon partial pressures. The entire vacuum housing can be baked with heating tapes; residual gas analysis using a high sensitivity quadrupole mass filter indicates major ion intensities at m/e 2, 18, and 28. In order to facilitate sample holder exchange without venting the sample chamber, the instrument includes a turbo pumped vacuum load-lock device having a base pressure in the 10^{-7} Torr range.

3. Mass Spectrometer

The secondary ion beam is separated from the primary beam by a 90° spherical condenser (ESA) having a bore machined in the outer plate for passage of the primary beam. Since its energy is much higher than that of the secondary beam, it experiences only a slight deflection on its passage through the lower part of the spherical condenser, which in turn can be compensated for by a corresponding predeflection in the set of deflection plates above. The ESA in combination with the secondary magnet form a stigmatically-imaging double-focussing (i.e. angular and energy focusing) mass spectrometer. The secondary beam is made parallel by the COALA lens, enters the ESA and forms an energy--dispersed intermediate focus at the exit of the ESA. The choice of the geometrical parameters is such that the energy dispersion at the intermediate focus is cancelled by the dispersion of the secondary magnet (see eq. 3 of ref. (72); mean radius of ESA = L = 12.0 cm; distance between plane of slits and apex of mean trajectory in magnetic field A = 14.0 cm). A continuous dynode electron multiplier is placed at the exit of the condenser field, and is used as a pulse counting energy monitor for the total sputtered negative-ion population. The energy spectrometer output is useful as a first stage check that

the secondary ion optics are adjusted properly for optimum pick-up before commencing work with the secondary magnet. With an energy stop of 3 mm width and 1000 V acceleration voltage, the transmitted energy band width is 25 eV. A Galileo model 4830 electron multiplier, operated in the pulse counting mode, serves for detection of the mass-analyzed negative secondary ions.

The instrument is equipped with an electronic aperture unit which controls gated counting of the secondary ion signal when rastering. Data obtained from microscopic inspection of a series of craters and line scans across an Au/Hf grid were used to construct an "xy raster" calibration curve having scan width as ordinate and raster plate deflection voltage as abscissa. The study indicated adjustable beam rastering is possible (at 5 kV accelerating voltage) up to 70 μm x 70 μm; the smallest area is governed, with its effect on detection sensitivities kept in mind (74), by the lowest practical beam size having adequate current and the general rule of maintaining a scan width-to-beam ratio of not less than 5. An optical photomicrograph of a 45 μm x 45 μm crater raster eroded at 100 lines/frame in a silicon matrix is presented in Fig. 11. An ion flux of approximately

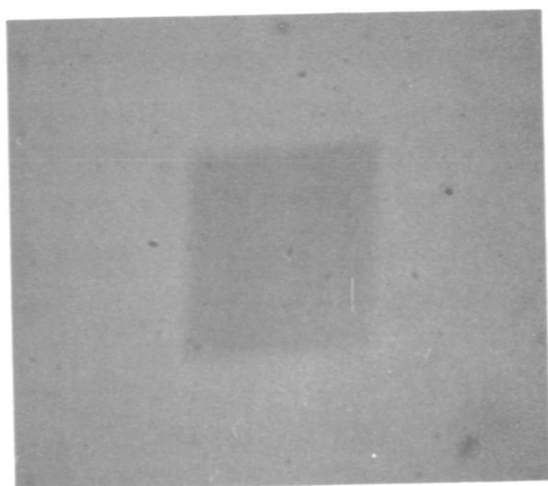

Fig. 11: Raster crater in silicon

2.6×10^{16} ions/cm^2 passed through this region. Although there is probably some neutral component to the ion beam at the sample, halos surrounding the crater have never been observed. To give an idea of the Cs^+ primary beam size achievable with the microprobe, Fig. 12 shows results of an X-line scan across an Au/Hf grid sample having Au bar

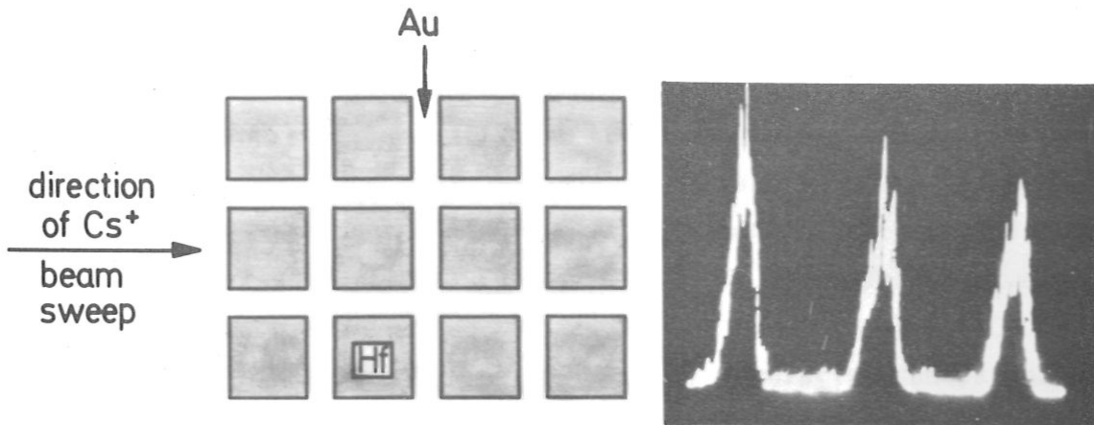

Fig. 12: Line scan along a Au/Hf grid deposit having 6.2 micron wide Au bars. $^{197}Au^{-}$ trace. The 6 keV Cs^{+} beam was swept across 3 such bars

width of 6.2 microns and Hf interspace width of 19.2 microns. The detected mass-analyzed secondary ion was $^{197}Au^{-}$, and the primary beam analog deflection circuitry was adjusted to sweep the Cs^{+} beam across three Au bars. A Cs^{+} primary beam with diameter in the few microns range was achieved.

B. Instrument Performance

The motive of the first SIMS experiment was to verify that the microprobe's combined objective and emission lens could pass the primary (+ charged) and secondary (- charged) beams coaxially in opposite directions. This experiment would prove to be the first time that the COALA lens fields were configured to focus and transmit ions of the said polarities. To this end, a set of metal samples was analyzed by secondary ion mass spectrometry at 6 keV Cs^{+} impact energy. Of interest was to record survey negative ion mass spectra from which relative intensities of negative ions could be compared. A static, mass-analyzed Cs^{+} beam of 20 μm diameter bombarded the sample at normal incidence so that current densities of 0.1 - 1.0 mA/cm^2 were maintained. Pressure in the sample chamber was $\sim 5 \times 10^{-8}$ Torr, with pumping provided only by the turbo pump; the LN_2 cryo baffle and Ti

sub pump were not in operation. Secondary ion spectra were collected by an X-Y recorder. Table 4 presents point analysis results from five unpolished metals (M). Cs bombardment, at the said pressure and energy, affords negative ion cluster and/or metal oxide formation. From a PAPYEX carbon matrix, homonuclear C_n^- clusters up to n = 9 were observed. It appears that for cases where metals such as Mo and Cr are found strongly oxidized, then detection of metal oxide species is more sensitive than M^-. Oxide formation ensues also from neutral cesium supply — Ar^+ bombardment, but polyatomic ion production is reported to be more dominant by direct Cs^+ bombardment (46). No MCs^- species were observed. Present in all mass spectra were non-analyte H^- and O^- ions; Figure 13 presents a mass spectrum of a GaP sample. Secondary negative ion count

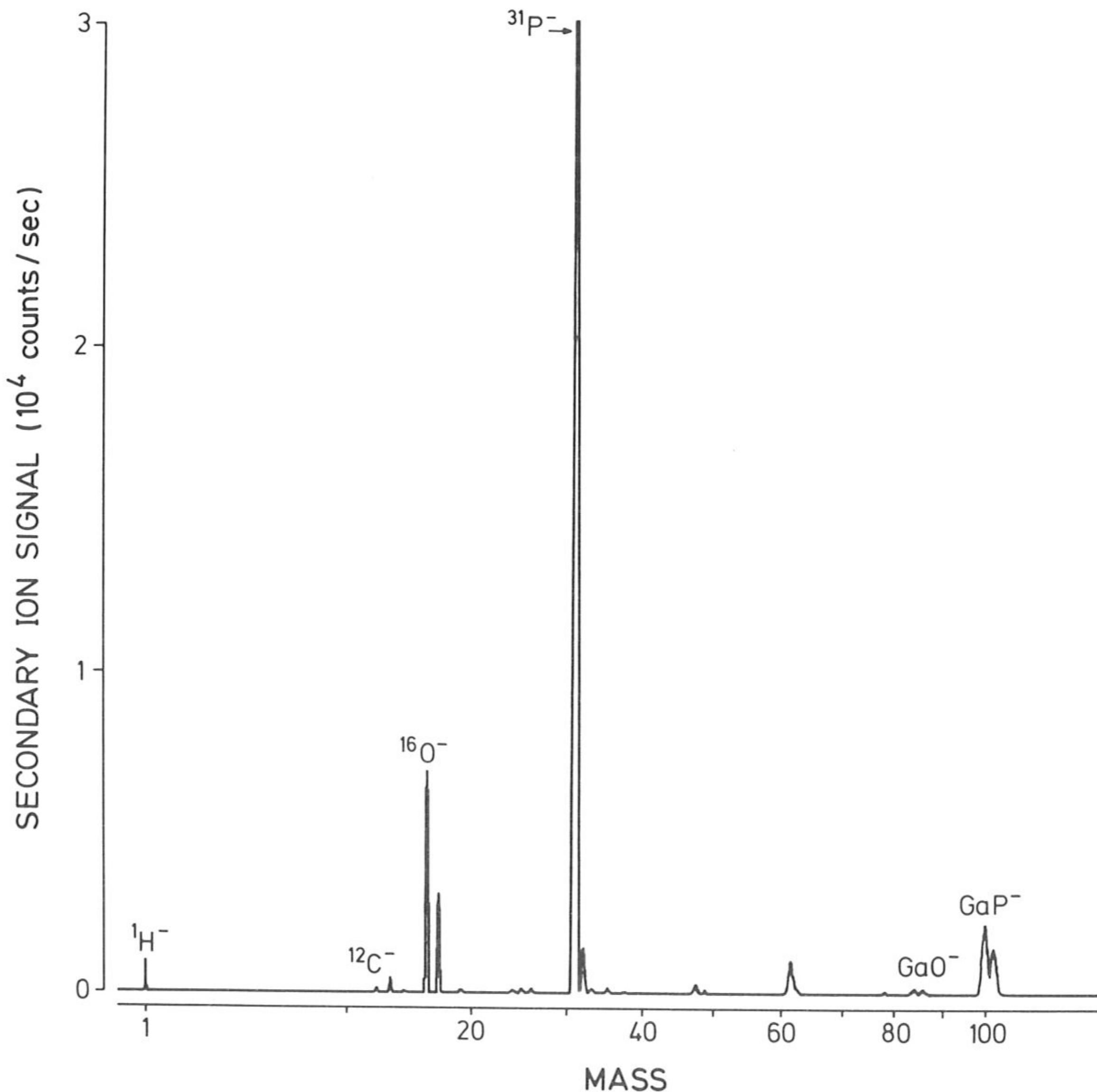

Fig. 13: Negative secondary ion mass spectrum of GaP. 6 keV Cs^+ bombardment. 3 x 10^4 cps full scale

Table 4: Normalized (relative) negative secondary-ion intensities associated with the metal M.

Sample	M^-	MO^-	MO_2^-	MO_3^-	M_2^-	M_2O^-	M_3^-	M_4^-	Other species
Al	1.00	8.30	2.16	0.11	0.33		0.05	0.04	
Si	1.00	0.04	0.85	0.49	0.01				$SiOH^-$
Mo	1.00	8.60	5.97	1.18					
Cu	1.00	0.43	0.10		0.01	0.01			$CuOH^-$, CuC_2^-, CuO_2H^-
Cr	1.00	4.27	1.52	0.14					

rates have been determined for the matrices studied, and from Table 5, one can get an idea of instrument sensitivity. Because the target current measured was not corrected for secondary electron emission, the relative ion yield values are probably larger than listed. When sputter-

Table 5: Relative secondary negative ion yields obtained on COALA ion microprobe (6 keV impact energy)

Element	Isotope	Detected counts per second/nA Cs^+ primary ion current
Al	27	4.7×10^3
Si	28	1.1×10^5
Cr	52	5.3×10^3
Cu	63	7.7×10^3
Mo	98	1.2×10^3

ing into a Si wafer, a count rate of 1.1×10^5 counts/sec·nA of incident Cs^+ was measured for $^{28}Si^-$. This compares within a factor of 4 - 10 to other Cs^+/SIMS machines described in references 11 and 24.

To evaluate the depth resolution achievable with the instrument, a tantalum oxide sample was studied which had a phosphorus-enriched zone nominally 50 Å thick inserted 1000 Å beneath the surface. Advantage was taken of the high negative ion yield of P under Cs^+ bombardment (2) (see Fig. 13); monitoring $^{31}P^-$, a value of 1.6×10^5 cps/nA of incident Cs^+ has been measured on the COALA machine. The ion microprobe was operated in a mode for small area depth profiling: an area of 19 µm x 19 µm was raster scanned at 100 lines/frame (time per full frame = 3.1 sec) using a 6 keV Cs^+ beam impinging 90^0 to the sample plane. The effective penetration rate was 0.4 Å/sec. The sharp interference colors in the Ta_2O_5 film could be directly viewed through the optical microscope. Figure 14 presents the MCA data plotter output of the phosphorus depth profile. As the mean projected range for a Cs particle, at the aforementioned energy and incident angle, is about 55 Å in this matrix, the peak of the ion damage distribution occurred

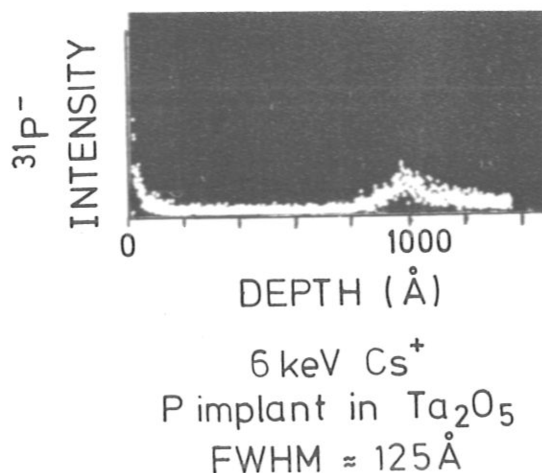

Fig. 14: Depth profile showing the ability of COALA to resolve thin layers beneath much thicker covering films

at a depth less than the location of the P insert. A value of 125 Å was found for the apparent full width at half maximum (FWHM) of the phosphorus layer. This value compares well with results (presented at the Tarrytown SIMS Workshop (75)) from other machines (Cameca IMS 300, ARL IMMA) using 5.5 - 8.5 KEV O_2^+ and detecting $^{31}P^+$. All results, including this work, report a phosphorus surface signal.

Effects of local current density at the sample (a 500 Å gold overlayer on silicon) are shown in Fig. 15. Cs^+-beam average current-density variations $\langle j_i \rangle$ were achieved by using the condenser lens to

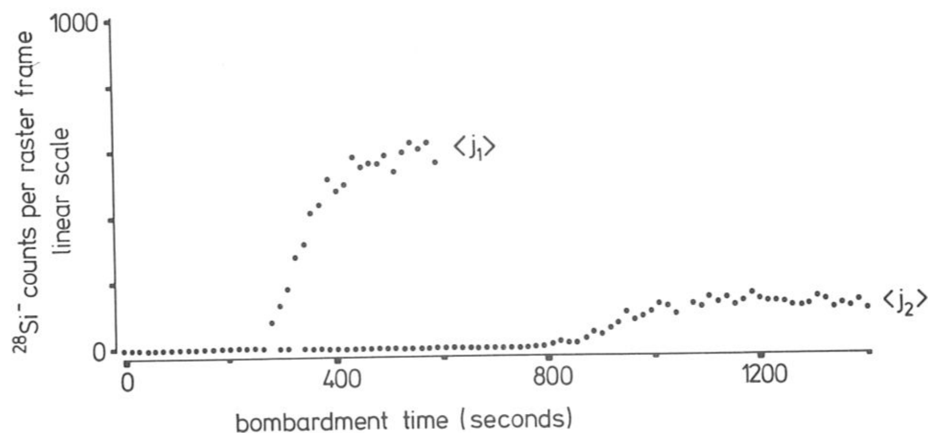

Fig. 15: $^{28}Si^-$ depth profile (from a silicon layer buried 500 Å under a film of Au) as a function of Cs^+ primary ion current density $\langle j_i \rangle \cdot \langle j_1 \rangle / \langle j_2 \rangle = 3.1$

vary the beam current at a fixed 19 μm x 19 μm scanned area. Using an electronic aperture gate of 7 % and scanning conditions of 1000 lines/frame and 15 sec/frame, the breakthrough time and amplitude of the $^{28}Si^-$ ion signal were measured at two values of target current differing in intensity by a factor of 3.1. Since fundamentals teach us that the measured secondary ion signal is proportional to the primary beam current (at a given area of irradiation), one expects the ion count from the two profiles to differ by a factor of 3.1. Experimentally, a value differing by 33 % was observed; that is, the "plateau" ion counts/raster frame from the depth profile at higher current density were a factor of 4.1 greater than at lower current density. The error may arise from matrix-related effects. Comparing the times at which the respective profiles first climb from baseline (i.e., the current density effect), the $\langle j_2 \rangle$ profile lagged the $\langle j_1 \rangle$ profile by a factor of 2.8.

A dual element depth profile of this sample is presented in Fig.16.

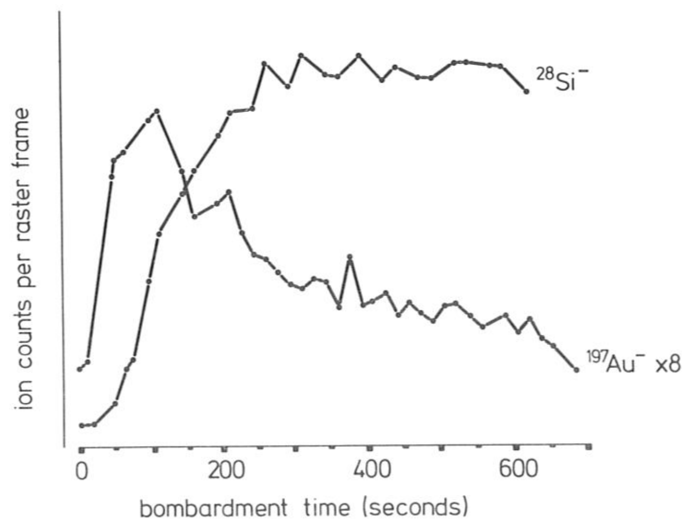

Fig. 16: Dual element depth profile

Because the secondary-ion magnetic spectrometer could not multichannel peak switch, two neighbouring sample spots had to be analyzed under identical experimental conditions. The interface shape appears smeared and although the abruptly rising profile of the $^{28}Si^-$ ion does not

hint at distortions, the Au signal indicates deviations from the otherwise expected sharp transition. The Au signal is enhanced somewhat approaching the interface; this effect has been observed by others in metal film - silicon systems (76) and is attributed to ion yield variance due to sputtering yield changes in the matrix (77). At the backside of the interface, insufficient crater edge rejection may have played a role in the slow decrease of the $^{197}Au^-$ signal, however, Williams has also measured such tailing and proposed that cascade mixing processes act to rebury much of the overlayer material (21). Non-uniform erosion due to cone formation would also tend to smear-out the profile.

As *per* design spec., secondary ion mass analysis is in a low resolution mode. Low resolution analysis can give rise to high background at a particular mass of interest if spectral interferences are present. Solutions are to either re-design the instrument for higher resolution or to select an isotope of the sought-for-constituent whose nominal, integer mass position is not masked. However, sensitivity loss due to isotopic abundance is a possibility, and some elements are monoisotopic. Another option to circumvent this problem is a choice of the secondary ion charge polarity. These points are illustrated in the probe studied in Fig. 17, which is a spectrum recorded at the start of depth profiling run of an ion-implanted sample

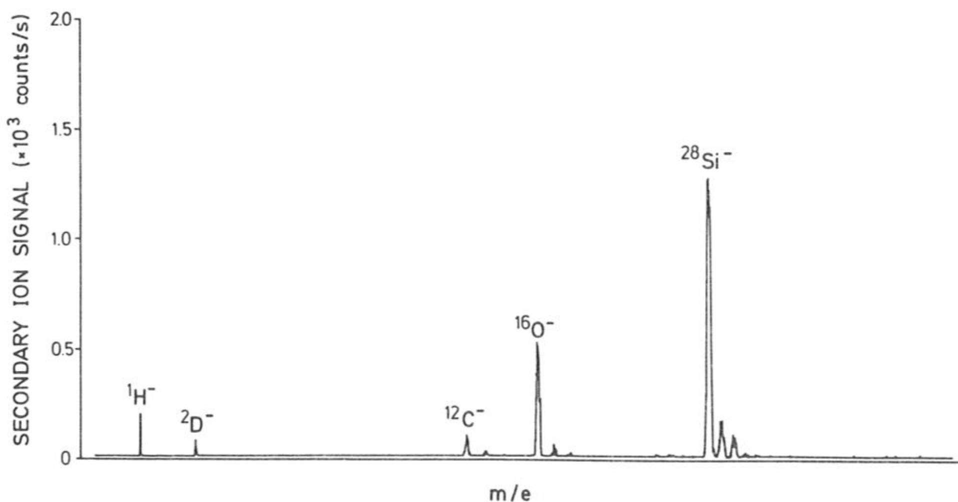

Fig. 17: Negative ion SIMS detection of implant species (D) in matrix (Si)

(deuterium in silicon). Analysis for deuterium at m/e 2 by positive ion SIMS may be complicated by the stable species H_2^+ (25), and would require a mass resolution in excess of 1000 for full differentiation, but the lack of stable H_2^- species gives a clean spectral position for negative ion spectroscopy.

Figure 18 shows the experimental depth profile. Its shape is not symmetrical Gaussian, but neither is the distribution calculated by

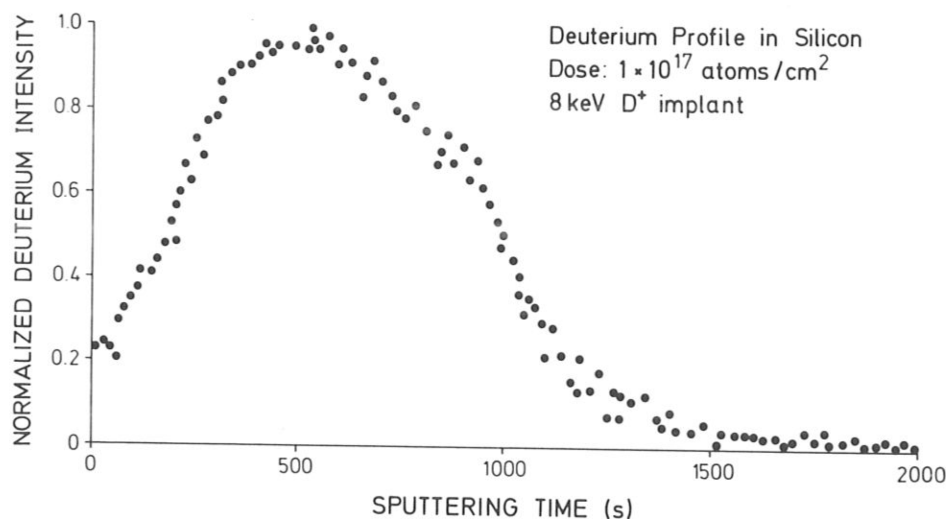

Fig. 18: Profile in-depth following $^2D^-$

computer using a TRIM program (78), which also gives a value of 1690 Å for the average depth (mean projected range) of the implantation distribution. Non-uniform sputter erosion or cratering effects may be responsible for the inflection seen in the trailing section of the profile, where profiling is done from higher concentration to lower concentration. Using a macroprobe type instrument, another laboratory has measured, for a 5 keV D^+ implant, a profile having nonsymmetrical shape with a finite surface D concentration (1/5 relative to peak concentration) (28). A strong near-surface signal is also seen in the Figure. For comparison, a second implant at lower dose (10^{15} at/cm^2) was studied. At equal sputtering current densities, best results were that the maxima of the two distributions coincided (in time) within 5 %. The peak count rate from the 10^{15} at/cm^2 sample was a factor of 104 less than the peak of the 10^{17} at/cm^2 sample.

V. REFERENCES

/1/ H. Liebl, Adv. Mass Spectrom. 7A, 807 (1978)
/2/ H.A. Storms, K.F. Brown, and J.D. Stein, Anal. Chem. 49, 2023 (1977)
/3/ V.E. Krohn, J.Appl.Phys. 33, 3523 (1962)
/4/ P. Vallerand and M. Baril, Int.J.Mass Spectrom.Ion.Phys. 24, 241 (1977)
/5/ H. Andersen and H. Bay, Chapter 4 of Sputtering by Particle Bombardment I, ed. by R. Behrisch, Springer-Verlag Heidelberg 1981, Vol. 47, p.145
/6/ M. Abdullayeva, A. Akukhanov, and U. Shamsiyev, in Ion Surface Interaction, Sputtering and Related Phenomena, ed. R. Behrisch, W. Heiland, W. Poschenrieder, P. Staib, H. Verbeek, Gordon and Breach Publ., London, 1973, p. 167
/7/ J.E. Chelgren, W. Katz, V. Deline, C.A. Evans, Jr., R. Blattner, and P. Williams, J.Vac.Sci.Tech. 16 (2), 324 (1979)
/8/ M. Bernheim, J. Rebière, and G. Slodzian, in Secondary Ion Mass Spectrometry: SIMS II, Springer-Verlag Series in Chemical Physics Series 9, 1980, p. 40
/9/ C.A. Andersen, Int.J.Mass Spectrom.Ion Phys. 3, 413 (1970)
/9a/ Y. Ueda and J. Okano, Mass Spectrom. 20 (3), 185 (1972)
/10/ E. Zandberg and N. Ionov, in Surface Ionization, Israel Program for Scientific Translations, Jerusalem, 1971, Chapter 12
/11/ P. Williams, R.K. Lewis, C.A. Evans,Jr., and P.R. Hanley, Anal.Chem., 49, 1399 (1977)
/12/ J. Pelletier, C. Pomot, and J. Cocogne, J.Appl.Phys. 50, 4517 (1979)
/13/ A. Lidow, J. Gibbons, V. Deline, and C.A. Evans,Jr., Appl.Phys.Lett. 32, 15 (1978)
/14/ A. Lidow, J. Gibbons, V. Delins, and C.A. Evans,Jr., Appl.Phys.Lett. 32, 149 (1978)
/15/ P. Williams and C.A. Evans,Jr., Appl.Phys.Lett. 30, 559 (1977)
/16/ A. Lidow, J. Gibbons, V. Deline, and C.A.Evans,Jr., Appl.Phys.Lett. 32, 572 (1978)
/17/ M. Tsai, B. Streetman, P. Williams, and C.A. Evans,Jr., Appl.Phys.Lett. 32, 144 (1978)
/18/ M. Tsai, D. Day, B. Streetman, P. Williams, and C.A.Evans,Jr., J.Appl.Phys. 50, 188 (1979)
/19/ G. Mezey, E. Kötal, T. Nagy, L. Lohner, A. Manuba, J. Gyulai, V. Deline, C.A.Evans,Jr., and R. Blattner, Nucl.Instrum.and Meth., 167, 279 (1979)
/20/ A. Lidow, J. Gibbons, V. Deline, and C.A.Evans,Jr., J.Appl.Phys. 51, 4130 (1980)
/21/ P. Williams, Appl.Phys.Lett. 36, 758 (1980)
/22/ H.A. Storms, Proc. 13th Microbeam Analysis Society Meeting, 1978, paper 7-A
/23/ C.W. Magee, W. Harrington, and R. Honig, Rev.Sci.Instrum. 49, 477 (1978)
/24/ C.W. Magee, J.Electrochem. Soc. 126, 660 (1979)
/25/ C.W. Magee and E. Botnick, J.Vac.Sci.Tech. 19, 47 (1981)
/26/ C.W. Magee, J.C. Bean, G. Foti, and J.M. Poate, Thin Solid Films 81, 1 (1981)
/27/ C.W. Magee, Appl.Phys.Lett. 37, 615 (1980)
/28/ C.W. Magee, S. Cohen, D. Voss, and D. Brice, Nucl.Instr.and Meth. 168, 383 (1980)
/29/ C.W. Magee, in Secondary Ion Mass Spectrometry: SIMS II, Springer-Verlag Series in Chemical Physics Series 9, 1980, p. 88
/30/ G. Clark, C. White, D. Allred, B. Appleton, C.W. Magee, and D.F. Carlson, Appl.Phys.Lett. 31, 582 (1977)
/31/ C.W. Magee, Int.Phys.Conf.Series #43 (Institut of Physics, London), 1979, Chapter 21, p. 693
/32/ D. Carlson and C.W. Magee, Appl.Phys.Lett. 33, 81 (1978)
/33/ S. Cohen, H. Dylla, W. Wampler, and C. Magee, J.Nucl.Mat. 93&94, 109 (1980)

/34/ P. Vallerand and M. Baril, Proc. 7th Int.Vac.Cong. and 3rd Int.Conf. Solid Surfaces, Vienna, 1977, p. 2569
/35/ M. Baril, 28th American Society for Mass Spectrometry (ASMS) Meeting, New York, New York, 1980, paper WAMP6
/36/ M. Baril, 27th American Society for Mass Spectrometry (ASMS) Meeting, Seattle, Wa., 1979, paper TPM088, p. 309
/37/ M. Baril and M. Babout, Proc. 1980 Vacuum Congress, Cannes, France, p.1334
/38/ R.W. Dreyfus, Appl.Phys.Lett. 36, 495 (1980)
/39/ R.W. Dreyfus, Appl.Phys.Lett. 38, 645 (1981)
/40/ T. Okutani, K. Shana, and R. Shimizu, in Secondary Ion Mass Spectrometry: SIMS II, Springer-Verlag Series in Chemical Physics Series 9, 1980, p. 186
/41/ N. Mueller and G. Hortig, IEEE Trans.Nucl.Sci., NS-16, 38 (1969)
/42/ F. Simondet, P. Dohony, and M. Decaesteker, Proc. 8th Int.Vac.Congress, Cannes, France, 1980, Vol. I: Thin Films, p. 275
/43/ S.A.E.S. Getters Sp.A., Milan, Italy, Technical brief disclosure
/44/ M. Bernheim and G. Slodzian, J. de Phys. (Lett.), 38L, 325 (1977)
/45/ M. Bernheim and G. Slodzian, Int.J.Mass Spectrom. Ion Phys. 20, 295 (1976)
/46/ M. Bernheim and G. Slodzian, paper presented at SIMS III Meeting, Budapest, August 31-September 4, 1981, abstract book p. 127
/47/ V.F. Krohn and G. Ringo, Appl.Phys.Lett. 27, 479 (1975)
/48/ L.W. Swanson, G. Schwind, and A. Bell, J.Appl.Phys. 51, 3453 (1980)
/49/ L.W. Swanson, G. Schwind, A.E. Bell, and J. Brady, J.Vac.Sci.Tech., 16, 1864 (1979)
/50/ R.L. Slinger, R.L, Kubena, R. Olney, J.Wand, and V. Wong, J.Vac.Sci.Tech., 16, 1610 (1979)
/51/ P. Prewett and D. Jefferies, Inst.Phys.Conf.Ser. #54 (Institut of London), 1981, p. 316
/52/ A. Dixon and A. von Engel, Inst.Phys.Conf.Ser. #54 (Institut of London), 1981, p. 292
/53/ P. Prewett and D. Jefferies, J.Phys.D: Appl.Phys. 13, 1747 (1980)
/54/ H. Kuwano, K. Yoshida, and S. Yamazaki, Jap.J.Appl.Phys. 19, L615 (1980)
/55/ K.L. Aitken and G. Mair, J.Phys. D: Appl.Phys. 13, 2165 (1980)
/56/ A. Wagner and T. Hall, J.Vac.Sci.Tech. 16, 1871 (1979)
/57/ A. Waugh, J.Phys.D: Appl.Phys. 13, L203 (1980)
/58/ K. Gamo, T. Ukegawa, Y. Inomoto, K. Ka, and S. Namba, Jap.J.Appl.Phys. 19, L595 (1980)
/59/ H. Liebl, Nucl.Instr.Meth. 187, 143 (1981)
/60/ Dubilier Scientific Ltd., Abingdon, England,Provisional Specification DS-5100
/61/ Vacuum Generators GmbH, Wiesbaden, West Germany, Technical Disclosure 8/80
/62/ F.G. Rüdenauer, P. Pollinger, H. Studnicka, H. Gnaser, W. Steiger, and M.J. Higatsberger, paper presented at SIMS III Meeting, Budapest, August 31-September 4, 1981, abstract book p. 39
/63/ L. Loeb, Rev.Sci.Instrum. 4, 486 (1933)
/64/ reference 10, Chapter 10
/65/ H. Liebl, in: "Secondary Ion Mass Spectrometry SIMS II", Springer-Verlag Series in Chemical Physics 9, Springer-Verlag Heidelberg-Berlin-New York, 1979, p. 176
/66/ B.L. Bentz and H. Liebl, paper presented at the International SIMS III Meeting, Budapest, August 31 - September 4, 1981, abstract book p. 13. To be published in book form by Springer-Verlag
/67/ S. Bosch and G. Kuskevics, Phys.Rev. 134 (5A), A 1356 (1964)
/68/ A.N. Broers, in Microprobe Analysis, ed. by C.A. Andersen, John Wiley + Son, New York, 1973, Chapter 3, p. 83
/69/ S. Hellier, report prepared for S.A.E.S. Getters S.p.A., Milan, Italy, "Measurement of Gaseous Impurities in Alkali Metal Vapor Generated by a Dispenser"
/70/ R. Clampitt and D. Jefferies, Nucl.Instr.Meth. 149, 739 (1978)

/71/ H.A. Storms, K.F. Brown, and J.D. Stein, Report on Second Japan-US Joint Seminar on SIMS, Takarazuka, Japan, October 23-27, 1978, p. 267

/72/ H. Liebl, Int.J.Mass Spectrom.Ion Phys. 6, 401 (1971)

/73/ H. Liebl, Vacuum, 22, 619 (1972)

/74/ T.A. Whatley, D.J. Comaford, J. Colby, and P. Miller, in "Surface Analysis Techniques for Metallurgical Applications", R.S.Carbonara and J.R. Cuthill, Eds., ASTM STP 596, Am.Soc. for Testing Mat., Philadelphia (1976), p. 114

/75/ C.A. Evans, B.N. Colby, G.L. Kearns, and W. Singer, Anal.Chem. 45, 398A (1973)

/76/ C.W. Magee, paper presented at the 1981 Ion Beam Analysis Conference, Sydney Australia

/77/ V.R. Deline, W. Katz, C.A. Evans, and P. Williams, Appl.Phys.Lett. 33, 932 (1978)

/78/ W. Eckstein, Max-Planck-Institut für Plasmaphysik, Report IPP 9/33, Oktober 1980